THE JOURNAL OF PHYSICAL CHEMISTRY C
A JOURNAL OF THE AMERICAN CHEMICAL SOCIETY

pubs.acs.org/JPCC

Article

Reversible Light-Induced Enhancement of Photoluminescence Lifetime and Intensity in Perovskite-Phase $CsPbI_3$ Nanocrystals

Published as part of The Journal of Physical Chemistry virtual special issue "Horst Weller Festschrift".

Michael K. Abney, Mokshin Suri, Tushti Shah, Francis Leonard Deepak, and Brian A. Korgel*

Cite This: *J. Phys. Chem. C* 2022, 126, 12712−12720

Read Online

ACCESS | Metrics & More | Article Recommendations | Supporting Information

ABSTRACT: Light-induced changes in photophysical and electronic properties in metal halide perovskites can affect their performance in photovoltaic devices, light-emitting diodes, and other applications. Here we reveal that light induces a slow, reversible enhancement in photoluminescence (PL) lifetime and intensity in films of perovskite-phase $CsPbI_3$ nanocrystals. When films of $CsPbI_3$ nanocrystals stored in air are photoexcited, their PL lifetime and intensity increase by as much as a factor of 5 over the course of 20−30 min. Several hours later, without additional light excitation, the initial PL lifetime and intensity return. Placing the films under vacuum or nitrogen for several minutes was also found to increase the PL lifetime and intensity. We propose a model of slow, humidity- and light-sensitive surface states in perovskite-phase $CsPbI_3$ nanocrystals.

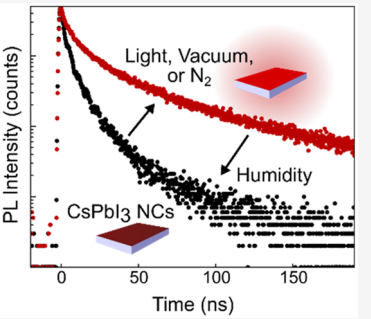

INTRODUCTION

Lead halide perovskite nanocrystals exhibit a variety of potentially useful properties, including size- and composition-tunable band gaps,[1−4] narrow photoluminescence (PL) emission line widths,[5−7] near-unity PL quantum yield (QY),[8−13] superfluorescence,[14] and tolerance to defects.[15−18] They have been used to fabricate optical detectors,[19−21] photovoltaic devices (PVs),[22−34] and light-emitting diodes (LEDs).[35−41] The performance and design of these devices depend on charge carrier recombination kinetics, which have been the focus of many studies. For example, time-resolved photoluminescence (trPL) spectroscopy measurements have shown that the radiative lifetimes of $CsPbX_3$ (X = Cl, Br, I) nanocrystals increase with decreasing temperature, which is unique among most semiconductor quantum dots and has been ascribed to a bright triplet state.[42]

Light-induced changes in the photophysical and electronic properties of metal halide perovskites can also occur. Tsai et al.[43] showed that thin films of formamidinium methylammonium cesium lead iodide ($FA_{0.7}MA_{0.25}Cs_{0.05}PbI_3$) in photovoltaic devices exhibited a 2-fold increase in PL intensity, a PL peak red-shift of about 5 nm, and an increase in open-circuit voltage over the course of about 120 min of 1 sun illumination. This light-induced response was attributed to an elongation of Pb−I bonds, although the details of these results and this mechanism are still under discussion.[44] The PL intensity and lifetime of metal halide perovskite nanocrystals are also known to be affected by surface chemistry.[8−10,13,15,45] Most commonly, photoexcitation can decrease the PL, as has been observed from $CsPbI_3$ nanocrystals under illumination.[46,47] For $CsPbBr_3$ nanocrystals under UV illumination, Ruan et al.[48] observed an increase in PL intensity and lifetime, and attributed this to self-passivation of halide vacancies. Zhang et al.[49] showed an increase in PL QY over the course of 5−10 min from $CsPbBr_3$ nanocrystals exposed to UV-NIR femtosecond laser pulses. There have been other reports of increased PL QY and lifetime from $CsPbBr_3$ nanocrystals following UV exposure, but all in conjunction with additional factors like annealing[50] or photoinduced morphology changes.[51] Seth et al.[52] reported significant increases in PL intensity over the course of several hours for $CsPbBr_3$ and $CsPbBr_2I$ nanocrystals, but with only minor increases in PL lifetime.

Here we show that PL lifetime and intensity of perovskite-phase $CsPbI_3$ nanocrystal films can slowly increase after an initial photoexcitation for approximately 20−30 min before eventually stabilizing. The PL quantum yield and lifetime can increase during this time by as much as a factor of 5. The increase in PL intensity and lifetime is reversible, and several hours after removing the light source, the initially short lifetime and lower PL intensity return. The nanocrystal films that exhibit this phenomenon are stored in air. By placing the $CsPbI_3$ nanocrystal films under vacuum or nitrogen in the dark, we found that a similar increase in PL lifetime and intensity was observed. These results point to the presence of slow

Received: June 21, 2022
Revised: July 9, 2022
Published: July 22, 2022

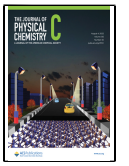

https://doi.org/10.1021/acs.jpcc.2c04305
J. Phys. Chem. C 2022, 126, 12712−12720

surface states in perovskite-phase $CsPbI_3$ nanocrystals mediated by humidity and light.

EXPERIMENTAL METHODS

Materials. Lead iodide (PbI_2, 99.999% (metals basis), Sigma-Aldrich), cesium carbonate (Cs_2CO_3, 99.9% (metals basis), Sigma-Aldrich), oleylamine ($C_{18}H_{35}NH_2$, OAm, technical grade, 70%, Sigma-Aldrich), oleic acid ($C_{18}H_{34}O_2$, OA, technical grade, 90%, Sigma-Aldrich), 1-octadecene (ODE, $C_{18}H_{36}$, technical grade, 90%, Sigma-Aldrich), methyl acetate ($C_3H_6O_2$, MeOAc, 99.5%, anhydrous, Sigma-Aldrich), hexane (>99%, anhydrous, Sigma-Aldrich), and toluene (>99%, anhydrous, Sigma-Aldrich) were used as received without further purification.

$CsPbI_3$ Nanocrystal Synthesis. Perovskite-phase $CsPbI_3$ nanocrystals were synthesized by using a procedure similar to Protesescu et al.[3,53,54] In a three-neck round-bottom flask, 407 mg (1.25 mmol) of Cs_2CO_3 and 1.25 mL of oleic acid were added to 20 mL of octadecene. On a Schlenk line, the mixture was stirred under vacuum for 20 min at room temperature. The temperature was then raised to 100 °C and stirred for 20 min. The flask was purged with nitrogen, and the temperature was raised to 150 °C until the mixture became clear. The temperature was reduced to 130 °C and left until ready to use later in the synthesis.

In a separate flask, 300 mg (0.651 mmol) of PbI_2 was added to 10 mL of octadecene and stirred under vacuum at 110 °C for 20 min. 1.5 mL each of oleylamine and oleic acid were combined, heated to 130 °C, and injected into the flask. The flask was kept stirring under vacuum until vapor was no longer observed to evolve from the mixture. The flask was placed under nitrogen, and the temperature was quickly raised to 165 °C. Once 165 °C was reached, 0.8 mL of the Cs−oleate mixture above was injected, followed by immediate quenching of the reaction with an ice bath.

Nanocrystals were purified by using hexane/MeOAc solvent/antisolvent precipitation, similar to Swarnkar et al.[32,53,54] MeOAc (25 mL) was added to the crude reaction product (a 2:1 MeOAc to reaction product ratio by volume), and the mixture was centrifuged at 7500 rpm (7232*g* rcf) for 5 min. The supernatant was discarded, and the precipitated nanocrystals were redispersed in 2 mL of hexane. After the addition of 2 mL of MeOAc, the mixture was immediately centrifuged at 7500 rpm for 5 min. The supernatant was discarded, and the precipitated nanocrystals were redispersed in 4 mL of hexane before finally centrifuging the dispersion at 5000 rpm (3214*g* rcf) for 2 min to remove insoluble reaction byproducts and poorly capped nanocrystals. The nanocrystals were stored as dispersions in sealed vials in the dark with refrigeration. A typical reaction yields ∼40 mg of nanocrystals.

Materials Characterization. For optical characterization, $CsPbI_3$ nanocrystals were dropcast or spin-coated from hexane or toluene dispersions onto soda lime glass microscope slides (Cardinal Health) to form films with thickness between 100 and 800 nm. The film thickness was measured by using a Keyence VK-X1100 optical profilometer. PL emission spectra were measured by using a Fluorolog-3 FL3−221 spectrofluorometer (Horiba Jobin Yvon) with 450 nm excitation wavelength and slit size of 5 nm for both excitation and emission. Time-resolved PL (trPL) data were measured on the Fluorolog-3 instrument with a FluoroHub-B time-correlated single photon counting (TCSPC) accessory. For trPL, photoexcitation was provided by a 442 nm wavelength NanoLED pulsed excitation source (pulse duration = 1.2 ns, repetition rate = 0.5−1 MHz). PL measurements under vacuum were taken by using a cryostat chamber (Janis Research Co.) and an Edwards 1.5 vacuum pump (1.1×10^{-3} Torr rated vacuum). UV−vis absorptance spectra were taken by using a Cary 5000 UV−vis−NIR spectrophotometer with an Agilent Technologies diffuse reflectance accessory. Absorptance, A, is the ratio of absorbed radiant energy to incident radiant energy, or $A = 1 -$ transmittance $-$ reflectance.

X-ray diffraction (XRD) was measured by using a Rigaku R-Axis Spider X-ray diffractometer with an image plate detector and Cu Kα radiation (λ = 1.54 nm). XRD data were collected for 10 min with 2 deg/s sample rotation, and the X-ray generator operated at 40 kV and 40 mA.

Transmission electron microscopy (TEM) images were acquired with an FEI Tecnai TEM at 80 kV accelerating voltage. TEM samples were made by dropcasting nanocrystals from a dilute dispersion in hexane onto a continuous carbon-coated copper mesh TEM grid (Electron Microscopy Sciences). High-angle annular dark-field scanning transmission electron microscopy (HAADF-STEM) was performed by using an FEI Titan G2 ChemiSTEM operated at 80 kV with a Cs probe corrector. For HAADF-STEM, the TEM grid was dipped in methyl acetate to remove excess ligand and carbon contamination. Prior to imaging, the TEM grids were loaded into the TEM and left undisturbed in a vacuum for several hours.

RESULTS

Figures 1a and 1b show transmission electron microscopy (TEM) and scanning transmission electron microscopy high angle annular dark field (STEM-HAADF) images of typical perovskite-phase $CsPbI_3$ nanocrystals nanocrystals used in the study. The nanocrystals have a cuboidal shape with an average edge length of 8.9 ± 2.0 nm. (Additional TEM images and a

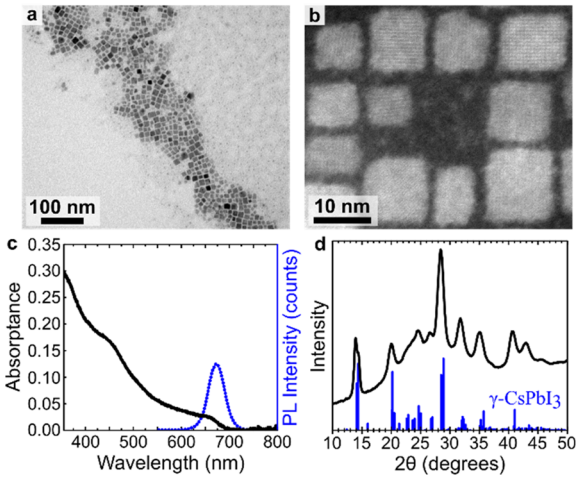

Figure 1. (a) TEM and (b) high-angle annular dark-field (HAADF) STEM images of the $CsPbI_3$ nanocrystals used in this study. (c) Room temperature absorptance and PL spectra of a $CsPbI_3$ nanocrystal film on glass (λ_{exc} = 450 nm). The absorptance was measured by using a diffuse reflectance integrating sphere to properly account for light scattering and reflection. (d) XRD of $CsPbI_3$ nanocrystals (black trace) compared to a calculated pattern (blue drop lines) for γ-orthorhombic $CsPbI_3$ with space group *Pbnm* (no. 62).[32,54,58]

https://doi.org/10.1021/acs.jpcc.2c04305
J. Phys. Chem. C 2022, 126, 12712−12720

histogram of particle sizes are provided as Supporting Information.) Figure 1d shows X-ray diffraction (XRD): the nanocrystals inhabit the perovskite, γ-orthorhombic phase of $CsPbI_3$.[55−59] Room temperature UV−vis absorptance and PL emission spectra from $CsPbI_3$ nanocrystals deposited on glass are shown in Figure 1c. The band-edge PL peak at 672 nm is typical for γ-$CsPbI_3$ nanocrystals.[3,4] PL quantum yields (QYs) of the $CsPbI_3$ nanocrystals dispersed in hexane range between 25 and 35%.[50]

Figure 2 shows room temperature PL and trPL of a film of $CsPbI_3$ nanocrystals that had been stored in air. The PL

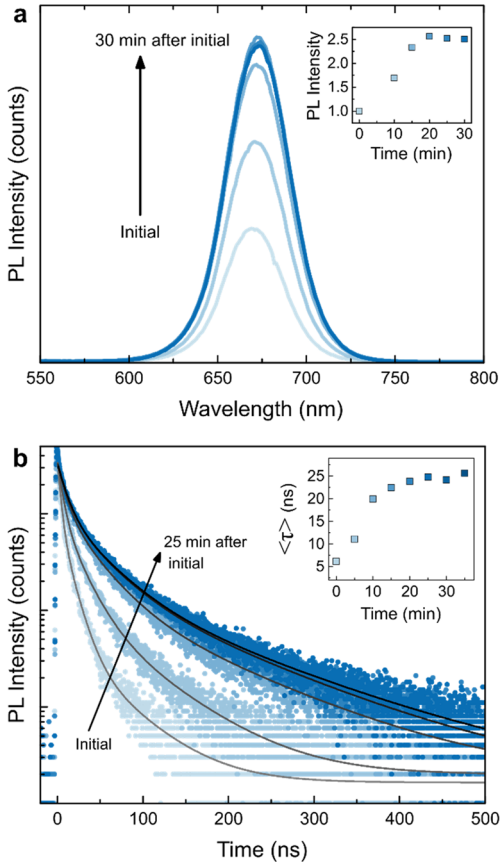

Figure 2. (a) Steady-state PL and (b) trPL of a $CsPbI_3$ nanocrystal film on glass in air with RH = 45−55% showing the increase in PL intensity and lifetime over time following the initial measurement. (a) PL measurements taken every 5 min over a 30 min period, with darker lines representing later measurements. The excitation wavelength (λ_{exc}) was 450 nm. Inset: time evolution of the integrated PL peak intensity normalized to its initial state after the PL is first measured. (b) trPL measurements taken every 5 min, with darker-colored data points representing later measurements. Each data set was fit with a triexponential decay (gray/black lines, see eq I). The excitation wavelength (λ_{exc}) was 442 nm. Inset: amplitude average lifetime $\langle\tau\rangle$ of each decay curve vs time after the initial measurement, where $\langle\tau\rangle = \sum a_i\tau_i$. For both sets of measurements, the excitation light was turned on only during measurement.

intensity and lifetime changes significantly for about 20 min before reaching a steady-state response. After leveling off, the PL intensity has increased by nearly a factor of 3, with a slight red-shift of 3 nm and increase in full width at half-maximum (FWHM) of about 3 nm. The PL lifetime can be quantified by fitting the trPL data with a triexponential decay:

$$I(t) = a_1 \exp\left(\frac{-t}{\tau_1}\right) + a_2 \exp\left(\frac{-t}{\tau_2}\right) + a_3 \exp\left(\frac{-t}{\tau_3}\right) \quad \text{(I)}$$

Similar to other reports of $CsPbX_3$ nanocrystals and films,[50−52,60−62] single- or biexponential decay functions do not accurately fit the data, except when the lifetimes were short—in our case, only during the initial trPL measurement. Once the lifetime increases, the triexponential fit is needed. The amplitude average PL lifetime, $\langle\tau\rangle = \sum a_i\tau_i$,[63] of the sample in Figure 2 (shown in the inset of Figure 2b) increased from 6.1 to 24.8 ns. Table 1 provides the fitting parameters used to obtain $\langle\tau\rangle$. The values of $\langle\tau\rangle$ lie within the range of values reported in the literature for $CsPbI_3$ nanocrystals.[3,32,60,64]

Table 1. Parameters Used to Fit Eq I to the trPL Data in Figure 2b and the Corresponding Amplitude verage Lifetime $\langle\tau\rangle$ (Lifetime Values in ns)

	time (min) after light exposure						
	0	5	10	15	20	25	30
τ_1	3.39	5.41	8.15	8.82	9.43	9.77	8.47
a_1	0.74	0.70	0.64	0.65	0.65	0.65	0.62
τ_2	11.9	19.2	31.3	35.2	35.7	38.1	34.4
a_2	0.25	0.27	0.31	0.30	0.29	0.29	0.31
τ_3	49.7	64.2	109	121	118	129	120
a_3	0.01	0.03	0.05	0.05	0.06	0.06	0.07
$\langle\tau\rangle$	6.09	11.05	19.96	22.44	23.83	24.76	24.15

We found that PL intensity and lifetime continued to gradually increase after the initial light exposure during a PL measurement, even without continuous illumination, as shown in Figure 2. The data in Figure 2 were acquired by measuring the PL every 5 min, without any light exposure between measurements. Regardless of when the subsequent measurements were taken, the initial photoexcitation kicks off a gradual, slow change in PL kinetics. This change in PL intensity and lifetime is reversible, however, and when the sample is stored in the dark for several hours, the initial (short) PL lifetime and intensity return. Typically, this would take about 12 h when the nanocrystals are placed in ambient air at about 45−55% relative humidity (RH). When the PL spectra and lifetime are measured again, the photoexcitation during the initial measurement reinitiates a rise in PL intensity and lifetime. XRD (Figure 3) showed that the increased PL intensity and lifetime are not related to any change in crystal structure.

When γ-$CsPbI_3$ nanocrystals are dispersed in a solvent, they do not show any light-induced changes in PL intensity and lifetime (see Figure S2 in the Supporting Information). The PL lifetime of $CsPbI_3$ nanocrystals dispersed in hexane was 13 ns, which is longer than the initial PL lifetime of the films (6 ns) and shorter than the steady-state lifetime observed after photoexcitation (24 ns). One other significant difference between nanocrystals dispersed in a solvent and those dried into films is that the PL rapidly deteriorated in the dispersions, with decreasing lifetime and intensity, most likely due to ligand desorption and degradation as the nanocrystals reverted to their equilibrium yellow, non-emitting orthorhombic δ-phase. As we have previously shown, ligand-stabilized γ-$CsPbI_3$ nanocrystals are quite stable in air, even under humid conditions.[54]

https://doi.org/10.1021/acs.jpcc.2c04305
J. Phys. Chem. C 2022, 126, 12712−12720

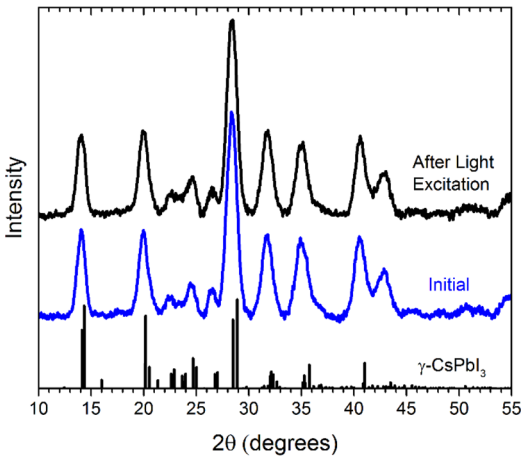

Figure 3. X-ray diffraction from a $CsPbI_3$ nanocrystal film before (black line) and after (blue line) an induced increase in PL intensity and lifetime by light excitation in air. The black drop lines correspond to calculated diffraction peaks for γ-orthorhombic $CsPbI_3$ with space group *Pbnm* (no. 62).[58]

To better understand the reversible light-induced enhancement of PL intensity and lifetime of γ-$CsPbI_3$ nanocrystals, we measured the PL under a variety of other environmental conditions. The PL intensity and lifetime also increased when the γ-$CsPbI_3$ nanocrystal film was placed under vacuum in the dark for several minutes. The black trace in Figure 4 shows

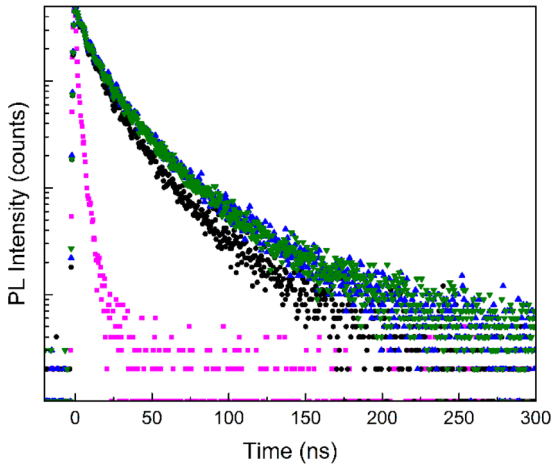

Figure 4. Time-resolved photoluminescence (trPL) of a γ-$CsPbI_3$ nanocrystal film under vacuum (black, blue, and green data points) compared to a γ-$CsPbI_3$ nanocrystal film in ambient air (magenta squares). For the film under vacuum, the initial measurement (black circles) was taken after leaving the sample under vacuum for 10 min. The traces shown in blue and green (up and down triangles, respectively) were taken 5 and 10 min after the initial measurement, respectively. The sample is illuminated only during the measurement by the excitation light source; otherwise, the sample is in the dark. The excitation wavelength (λ_{exc}) is 442 nm.

trPL data for a γ-$CsPbI_3$ nanocrystal film after being held under vacuum for 10 min. The magenta trace in Figure 4 shows the trPL data from a film without this vacuum treatment. The initial PL lifetime is significantly longer for the film placed under vacuum. The green trace in Figure 4 shows the trPL data measured 10 min after the first PL measurement for the film that had been placed under vacuum. There is still an increase in PL lifetime, but it is less pronounced and reaches steady state after only 5 min. After placing the film back into ambient air, the PL intensity and lifetime returned to their low values after about 12 h. Figure 5 shows a plot of $\langle\tau\rangle$ for a γ-$CsPbI_3$ nanocrystal film as it changes under vacuum, in air, and after photoexcitation. Both vacuum- and light-induced changes are reversible.

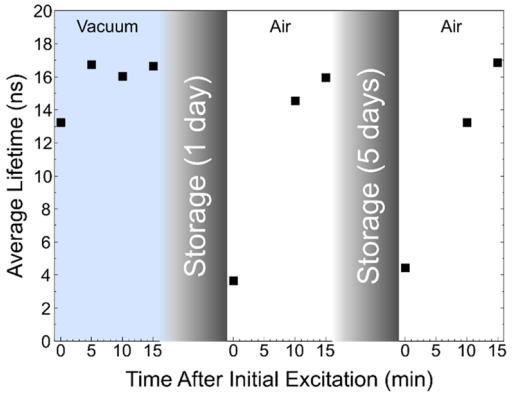

Figure 5. Change in average PL lifetime $\langle\tau\rangle$ of a γ-$CsPbI_3$ nanocrystal film after light excitation followed by storage in humid air (45−55% RH) at room temperature. The data points labeled "Vacuum" were obtained after the film had been placed under vacuum for 10 min and then measured under vacuum. The trPL data labeled "Air" were taken in ambient air. The sample is illuminated only during the measurement by the excitation light source; otherwise, the sample is in the dark. The excitation wavelength (λ_{exc}) is 442 nm.

We also found that γ-$CsPbI_3$ nanocrystal films placed under nitrogen before measuring the PL had a higher PL intensity and longer lifetime. After being stored for 1 h under nitrogen in the dark, the PL lifetime of the film was relatively long (15 ns) (see Figure S3). These films again revert back to lower PL intensity and shorter lifetimes when returned to ambient air (45−55% RH) for more than 12 h. The effects of the vacuum and nitrogen environments indicate that moisture plays a role in these reversible changes in PL intensity and lifetime.

Figure 6 shows the PL lifetime of films stored in air at 15% RH and 55% RH after the PL lifetime had been enhanced by light excitation. After 24 h, the PL lifetime of the film stored in 55% RH had dropped back to its initially short value, while the lifetime of the film stored in 15% RH remained slightly longer. Films took longer to recover their lower lifetime and intensity when stored in air with lower humidity. When the film was stored in nitrogen, it exhibited no decrease in PL lifetime or intensity after 24 h.

$CsPbI_3$ nanocrystal films were completely unstable under conditions of very high humidity (>90% RH) and turned yellow after about 12 h. Humidity is well-known for its role in destabilizing the black perovskite phase of $CsPbI_3$ by catalyzing the phase change to the equilibrium yellow, orthorhombic δ-phase.[54,58,59,65] Figure 7 shows XRD from a $CsPbI_3$ nanocrystal film that had been stored in air for 12 h at >90% RH and transformed to the equilibrium, non-perovskite δ-orthorhombic crystal phase. It should be noted that these transformed films look completely yellow to the eye but can still exhibit measurable PL from the residual γ-orthorhombic phase in the film. The PL lifetimes of these yellow films vary widely and depend on how much γ-$CsPbI_3$ is still present.

https://doi.org/10.1021/acs.jpcc.2c04305
J. Phys. Chem. C 2022, 126, 12712−12720

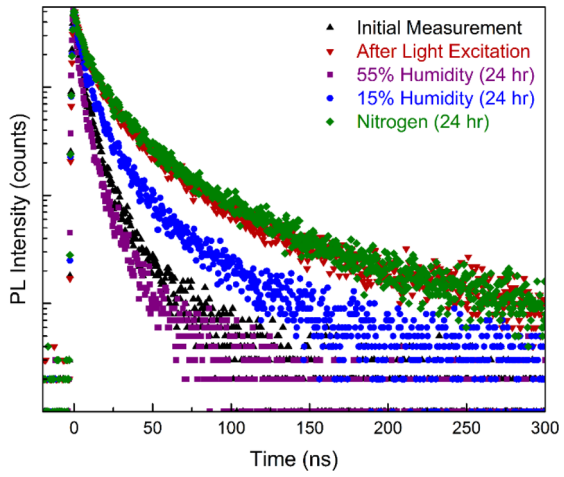

Figure 6. trPL of γ-$CsPbI_3$ nanocrystal films that had been photoexcited to induce an increase in PL lifetime and then stored under various conditions. Black triangles show the initial trPL of a film that had been stored in air, and red triangles show the trPL after light excitation, which exhibits the longest PL lifetime. The purple squares and blue circles show trPL data for films that were stored at 55 and 15% relative humidity, respectively, for 24 h. When the film was stored under nitrogen (green diamonds), there was no decrease in PL lifetime after 24 h. These measurements were taken in ambient air at 45−55% relative humidity with an excitation wavelength (λ_{exc}) of 442 nm.

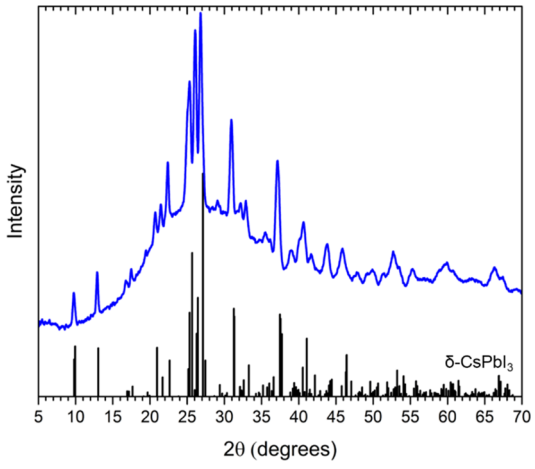

Figure 7. X-ray diffraction from a $CsPbI_3$ nanocrystal film on glass after 24 h in air at 90% RH (blue line). The nanocrystals have degraded to the yellow δ-orthorhombic phase from the initial black γ-orthorhombic phase. The reference of black drop lines are calculated diffraction peaks for δ-orthorhombic phase $CsPbI_3$ (PDF #01-074-1970).

DISCUSSION

Light-induced increases in PL intensity and lifetime have also been observed in the hybrid organic−inorganic perovskites, methylammonium lead iodide ($CH_3NH_3PbI_3$, MAPbI),[66−71] $MAPbBr_3$,[72,73] and $MAPb(I_{0.5}Br_{0.5})_3$.[74] Brenes et al.[69] proposed that photoinduced passivation of traps related to halide vacancies accounted for their observation of a gradual increase in PL from MAPbI films under continuous illumination. In MAPbI, vacancies can be filled by superoxide ions (O_2^-) formed by the interaction of oxygen and photoexcited electrons.[69,75−78] The light-induced changes that we observe in γ-$CsPbI_3$ nanocrystal films may also involve a similar oxygen passivation process; however, a mechanism that only considers oxygen cannot explain the increase in PL lifetime observed when films were placed under vacuum or nitrogen or the significant influence of humidity on the rate of the PL intensity and lifetime changes. In the case of γ-$CsPbI_3$ nanocrystal films, water must also be involved.

The PL QY and PL lifetime, τ_{PL}, are related to the radiative lifetime, τ_r, and the radiative and nonradiative electron−hole recombination rates, k_r and k_{nr}: $QY = k_r/(k_r + k_{nr}) = \tau_{PL}/\tau_r$.[79,80] The absorptance profile of the nanocrystal films did not change after illumination (see Figure S4), indicating that the amount of light absorbed by the nanocrystals does not change. Because similar enhancements are observed for both the QY and τ_{PL}, it is the change in nonradiative recombination that is responsible for the increased PL intensity and lifetime of the γ-$CsPbI_3$ nanocrystal films. We propose that the association of adsorbed water with the $CsPbI_3$ surface create slow surface states, or traps, that induce nonradiative recombination in the films.

The hydrophobic capping ligands help stabilize the γ-phase by preventing water vapor from reaching the crystal surface.[54] However, the ligands cannot completely passivate all of the dangling bonds presented by atoms at the nanocrystal surface because of the steric hindrance between neighboring alkyl chains.[81] It is known that water can interact with surface defects on the surface of lead halide perovskites and induce halide vacancies.[82−84] Liu et al.[85] showed that oxygen can passivate halide vacancies in $CsPbI_2Br$ and speculated that a decrease in exposed halide vacancies limits the adsorption of water. It is possible that both halide vacancies and water adsorption are involved in the formation of slow surface trap states on γ-$CsPbI_3$ nanocrystals. Filling of halide vacancies by oxygen and photoexcited electrons could then lead to the PL increase under light excitation that we observed.

According to our model, the rate of nonradiative electron−hole recombination can be reduced by either (1) the removal of adsorbed water and elimination of the trap states under vacuum or nitrogen or (2) the elimination of the surface trap states by a light-induced process involving photoexcited charge carriers, oxygen, and/or adsorbed water. To calculate the characteristic time or rate of deactivation of surface trap states following light excitation in air, we considered these distinct surface traps as dynamic PL quenchers and used kinetic equations to correlate the concentration of active surface traps to the measured PL lifetimes. In the presence of the quencher or surface trap, T, caused by the interaction of water with the perovskite surface, excited electrons can decay by the following steps illustrated in Figure 8:

$$S^* \xrightarrow{k_r} S + h\nu \quad (1)$$

$$S^* \xrightarrow{k_{nr}} S + \text{heat} \quad (2)$$

$$S^* + T \xrightarrow{k_T} S + T + \text{heat} \quad (3)$$

where S* and S are the excited and ground states, respectively, and k_T is the rate of nonradiative electron−hole recombination associated with the traps. Once the sample has been photoexcited

$$-\frac{d[S^*]}{dt} = k_r[S^*] + k_{nr}[S^*] + k_T[T][S^*] \quad (4)$$

Solving this differential equation gives

https://doi.org/10.1021/acs.jpcc.2c04305
J. Phys. Chem. C 2022, 126, 12712−12720

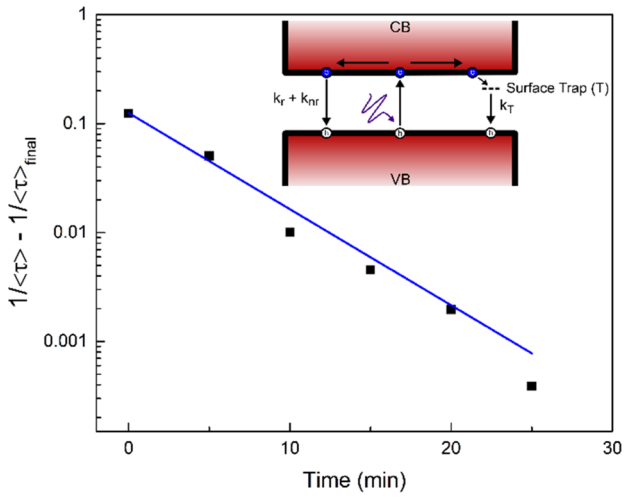

Figure 8. Plot of $1/\langle\tau\rangle - 1/\langle\tau\rangle_{final}$ vs time after initial photoexcitation for the data shown in Figure 2. $\langle\tau\rangle_{final}$, the steady-state (maximum) average lifetime of this sample, was taken to be 25 ns based on the values in Table 1. The best fit of eq 10 to the data (blue line) gives a value of the characteristic time for deactivation or elimination of slow surface trap states of τ_d = 4.9 min.

$$[S^*] = Ae^{-(k_r+k_{nr}+k_r[T])t} \quad (5)$$

to provide an expression for the PL lifetime in the presence of surface traps with a concentration of [T]:

$$\tau = \frac{1}{k_r + k_{nr} + k_T[T]} \quad (6)$$

In the absence of the surface traps, the PL lifetime (τ_0) is given by

$$\tau_0 = \frac{1}{k_r + k_{nr}} \quad (7)$$

From the ratio of the lifetimes in the absence and presence of the surface traps, a form of the Stern–Volmer equation is obtained:[80]

$$\frac{\tau_0}{\tau} = \frac{k_r + k_{nr} + k_T[T]}{k_r + k_{nr}} = 1 + \tau_0 k_T[T] \quad (8)$$

Rearranging this equation shows that [T] is related to the measured PL lifetimes according to

$$[T] = \frac{1}{k_T}\left(\frac{1}{\tau} - \frac{1}{\tau_0}\right) \quad (9)$$

The concentration of surface trap states [T] is proportional to $1/\tau - 1/\tau_0$. The PL lifetime in the absence of the trap states, τ_0, can be taken as the steady-state τ_{PL}, or τ_{final}, reached by the sample after photoexcitation. A first-order kinetic equation for the surface trap deactivation or elimination process, with trap state concentration [T] substituted by $1/\tau - 1/\tau_{final}$, yields

$$\frac{1}{\tau} - \frac{1}{\tau_{final}} = Ae^{-t/\tau_d} \quad (10)$$

where τ is taken as the amplitude average PL lifetime, $\langle\tau\rangle$, measured at time t after the initial excitation and τ_d is the characteristic time (inverse rate) of the deactivation or elimination of surface trap states caused by the interaction of water with the perovskite surface. Figure 8 shows the PL lifetime data from Figure 2 replotted to determine the characteristic time for deactivation or elimination of surface trap states, τ_d, which for this sample is 4.9 min. The photoinduced elimination of these trap states is a slow, reversible process. Although slow surface states on metal halide perovskites have not been previously identified, slow surface states are well-known for other semiconductors, such as Ge.[86] When the nanocrystal film is returned to humid air, the slow surface traps are reactivated by adsorbed water and the PL lifetime reverts back to the initially short values.

CONCLUSIONS

Here, we reveal the presence of humidity-sensitive slow surface states in γ-$CsPbI_3$ nanocrystals. The PL intensity and lifetime of γ-$CsPbI_3$ nanocrystals in films can change significantly after light excitation in a PL measurement, increasing by as much as a factor of 5 over the course of 20 min. These changes are reversible in a humid environment. Slow surface states are well known to occur in other semiconductors and are typically associated with reversibly bonded chemical species on the semicondcutor surface.[86] We propose that the slow surface states of the γ-$CsPbI_3$ nanocrystals affect only the nonradiative electron–hole recombination rates and are photosensitive. Passivation of the surface trap states can occur either through the removal of water interacting with the nanocrystal surface or by a slow light-activated process.

The sensitivity of optical properties to the combination of light and environmental moisture might be related to the fact that the perovskite phase of $CsPbI_3$ nanocrystals at room temperature is a metastable phase which is quite sensitive to moisture.[54,58,59] Further study is needed to delineate additional details concerning the reversible enhancement in PL intensity and lifetime of $CsPbI_3$ nanocrystal films. Light-intensity-dependent studies, for example, might provide more information about the kinetics of the surface interaction process and the role of trap filling. Our results highlight the complex optoelectronic behavior of $CsPbI_3$ nanocrystals and provide a better understanding of these materials with which to guide strategies for improving the performance and stability of inorganic perovskite devices.

ASSOCIATED CONTENT

Supporting Information

The Supporting Information is available free of charge at https://pubs.acs.org/doi/10.1021/acs.jpcc.2c04305.

Histogram of nanocrystal size distribution; trPL of nanocrystals dispersed in hexane; trPL of nanocrystal films with and without nitrogen exposure; absorptance spectra of $CsPbI_3$ nanocrystal films before and after the photoinduced PL increase (PDF)

AUTHOR INFORMATION

Corresponding Author

Brian A. Korgel − *McKetta Department of Chemical Engineering and Texas Materials Institute, The University of Texas at Austin, Austin, Texas 78712-1062, United States;* orcid.org/0000-0001-6242-7526; Phone: +1-512-471-5633; Email: korgel@che.utexas.edu

Authors

Michael K. Abney − *McKetta Department of Chemical Engineering and Texas Materials Institute, The University of*

Texas at Austin, Austin, Texas 78712-1062, United States; orcid.org/0000-0003-4155-2381

Mokshin Suri − *McKetta Department of Chemical Engineering and Texas Materials Institute, The University of Texas at Austin, Austin, Texas 78712-1062, United States;* orcid.org/0000-0003-0398-5725

Tushti Shah − *McKetta Department of Chemical Engineering and Texas Materials Institute, The University of Texas at Austin, Austin, Texas 78712-1062, United States;* orcid.org/0000-0002-7334-1979

Francis Leonard Deepak − *Nanostructured Materials Group, International Iberian Nanotechnology Laboratory, Braga 4715-330, Portugal;* orcid.org/0000-0002-3833-1775

Complete contact information is available at: https://pubs.acs.org/10.1021/acs.jpcc.2c04305

Notes

The authors declare no competing financial interest.

■ ACKNOWLEDGMENTS

Funding of this research was provided by the Robert A. Welch Foundation (F-1464), the UT|Portugal program, and the National Science Foundation through the Industry/University Cooperative Research Center on Next Generation Photovoltaics (IIP-1540028 and IIP-1822206) and the Center for Dynamics and Control of Materials (CDCM) Materials Research Science and Engineering Center (MRSEC) (DMR-1720595). F.L.D. acknowledges the Project CASOLEM (028917) "Correlated Analysis of Inorganic Solar Cells in and outside an Electron Microscope", co-funded by FCT and the ERDF through COMPETE2020.

■ REFERENCES

(1) Lignos, I.; Morad, V.; Shynkarenko, Y.; Bernasconi, C.; Maceiczyk, R. M.; Protesescu, L.; Bertolotti, F.; Kumar, S.; Ochsenbein, S. T.; Masciocchi, N.; et al. Exploration of Near-Infrared-Emissive Colloidal Multinary Lead Halide Perovskite Nanocrystals Using an Automated Microfluidic Platform. *ACS Nano* **2018**, *12*, 5504−5517.

(2) Nedelcu, G.; Protesescu, L.; Yakunin, S.; Bodnarchuk, M. I.; Grotevent, M. J.; Kovalenko, M. V. Fast Anion-Exchange in Highly Luminescent Nanocrystals of Cesium Lead Halide Perovskites ($CsPbX_3$, X = Cl, Br, I). *Nano Lett.* **2015**, *15*, 5635−5640.

(3) Protesescu, L.; Yakunin, S.; Bodnarchuk, M. I.; Krieg, F.; Caputo, R.; Hendon, C. H.; Yang, R. X.; Walsh, A.; Kovalenko, M. V. Nanocrystals of Cesium Lead Halide Perovskites ($CsPbX_3$, X = Cl, Br, and I): Novel Optoelectronic Materials Showing Bright Emission with Wide Color Gamut. *Nano Lett.* **2015**, *15*, 3692−3696.

(4) Akkerman, Q. A.; D'Innocenzo, V.; Accornero, S.; Scarpellini, A.; Petrozza, A.; Prato, M.; Manna, L. Tuning the Optical Properties of Cesium Lead Halide Perovskite Nanocrystals by Anion Exchange Reactions. *J. Am. Chem. Soc.* **2015**, *137*, 10276−10281.

(5) Huang, H.; Susha, A. S.; Kershaw, S. V.; Hung, T. F.; Rogach, A. L. Control of Emission Color of High Quantum Yield $CH_3NH_3PbBr_3$ Perovskite Quantum Dots by Precipitation Temperature. *Adv. Sci.* **2015**, *2*, 1500194.

(6) Yakunin, S.; Protesescu, L.; Krieg, F.; Bodnarchuk, M. I.; Nedelcu, G.; Humer, M.; De Luca, G.; Fiebig, M.; Heiss, W.; Kovalenko, M. V. Low-Threshold Amplified Spontaneous Emission and Lasing from Colloidal Nanocrystals of Caesium Lead Halide Perovskites. *Nat. Commun.* **2015**, *6*, 8056.

(7) Rainò, G.; Nedelcu, G.; Protesescu, L.; Bodnarchuk, M. I.; Kovalenko, M. V.; Mahrt, R. F.; Stöferle, T. Single Cesium Lead Halide Perovskite Nanocrystals at Low Temperature: Fast Single-Photon Emission, Reduced Blinking, and Exciton Fine Structure. *ACS Nano* **2016**, *10*, 2485−2490.

(8) Pan, J.; Shang, Y.; Yin, J.; De Bastiani, M.; Peng, W.; Dursun, I.; Sinatra, L.; El-Zohry, A. M.; Hedhili, M. N.; Emwas, A.-H.; et al. Bidentate Ligand-Passivated $CsPbI_3$ Perovskite Nanocrystals for Stable Near-Unity Photoluminescence Quantum Yield and Efficient Red Light-Emitting Diodes. *J. Am. Chem. Soc.* **2018**, *140*, 562−565.

(9) Ahmed, T.; Seth, S.; Samanta, A. Boosting the Photoluminescence of $CsPbX_3$ (X = Cl, Br, I) Perovskite Nanocrystals Covering a Wide Wavelength Range by Postsynthetic Treatment with Tetrafluoroborate Salts. *Chem. Mater.* **2018**, *30*, 3633−3637.

(10) Koscher, B. A.; Swabeck, J. K.; Bronstein, N. D.; Alivisatos, A. P. Essentially Trap-Free $CsPbBr_3$ Colloidal Nanocrystals by Postsynthetic Thiocyanate Surface Treatment. *J. Am. Chem. Soc.* **2017**, *139*, 6566−6569.

(11) Liu, F.; Zhang, Y.; Ding, C.; Kobayashi, S.; Izuishi, T.; Nakazawa, N.; Toyoda, T.; Ohta, T.; Hayase, S.; Minemoto, T.; et al. Highly Luminescent Phase-Stable $CsPbI_3$ Perovskite Quantum Dots Achieving Near 100% Absolute Photoluminescence Quantum Yield. *ACS Nano* **2017**, *11*, 10373−10383.

(12) Milstein, T. J.; Kroupa, D. M.; Gamelin, D. R. Picosecond Quantum Cutting Generates Photoluminescence Quantum Yields Over 100% in Ytterbium-Doped $CsPbCl_3$ Nanocrystals. *Nano Lett.* **2018**, *18*, 3792−3799.

(13) Li, F.; Liu, Y.; Wang, H.; Zhan, Q.; Liu, Q.; Xia, Z. Postsynthetic Surface Trap Removal of $CsPbX_3$ (X = Cl, Br, or I) Quantum Dots via a ZnX_2/Hexane Solution toward an Enhanced Luminescence Quantum Yield. *Chem. Mater.* **2018**, *30*, 8546−8554.

(14) Rainò, G.; Becker, M. A.; Bodnarchuk, M. I.; Mahrt, R. F.; Kovalenko, M. V.; Stöferle, T. Superfluorescence from Lead Halide Perovskite Quantum Dot Superlattices. *Nature* **2018**, *563*, 671−675.

(15) Nenon, D. P.; Pressler, K.; Kang, J.; Koscher, B. A.; Olshansky, J. H.; Osowiecki, W. T.; Koc, M. A.; Wang, L.-W.; Alivisatos, A. P. Design Principles for Trap-Free $CsPbX_3$ Nanocrystals: Enumerating and Eliminating Surface Halide Vacancies with Softer Lewis Bases. *J. Am. Chem. Soc.* **2018**, *140*, 17760−17772.

(16) Akkerman, Q. A.; Rainò, G.; Kovalenko, M. V.; Manna, L. Genesis, Challenges and Opportunities for Colloidal Lead Halide Perovskite Nanocrystals. *Nat. Mater.* **2018**, *17*, 394−405.

(17) Kang, J.; Wang, L.-W. High Defect Tolerance in Lead Halide Perovskite $CsPbBr_3$. *J. Phys. Chem. Lett.* **2017**, *8*, 489−493.

(18) Huang, H.; Bodnarchuk, M. I.; Kershaw, S. V.; Kovalenko, M. V.; Rogach, A. L. Lead Halide Perovskite Nanocrystals in the Research Spotlight: Stability and Defect Tolerance. *ACS Energy Lett.* **2017**, *2*, 2071−2083.

(19) Ramasamy, P.; Lim, D.-H.; Kim, B.; Lee, S.-H.; Lee, M.-S.; Lee, J.-S. All-Inorganic Cesium Lead Halide Perovskite Nanocrystals for Photodetector Applications. *Chem. Commun.* **2016**, *52*, 2067−2070.

(20) Chen, Q.; Wu, J.; Ou, X.; Huang, B.; Almutlaq, J.; Zhumekenov, A. A.; Guan, X.; Han, S.; Liang, L.; Yi, Z.; et al. All-Inorganic Perovskite Nanocrystal Scintillators. *Nature* **2018**, *561*, 88−93.

(21) Yakunin, S.; Benin, B. M.; Shynkarenko, Y.; Nazarenko, O.; Bodnarchuk, M. I.; Dirin, D. N.; Hofer, C.; Cattaneo, S.; Kovalenko, M. V. High-Resolution Remote Thermometry and Thermography Using Luminescent Low-Dimensional Tin-Halide Perovskites. *Nat. Mater.* **2019**, *18*, 846−852.

(22) Ling, X.; Zhou, S.; Yuan, J.; Shi, J.; Qian, Y.; Larson, B. W.; Zhao, Q.; Qin, C.; Li, F.; Shi, G.; et al. 14.1% $CsPbI_3$ Perovskite Quantum Dot Solar Cells via Cesium Cation Passivation. *Adv. Energy Mater.* **2019**, *9*, 1900721.

(23) Yuan, J.; Ling, X.; Yang, D.; Li, F.; Zhou, S.; Shi, J.; Qian, Y.; Hu, J.; Sun, Y.; Yang, Y.; et al. Band-Aligned Polymeric Hole Transport Materials for Extremely Low Energy Loss α-$CsPbI_3$ Perovskite Nanocrystal Solar Cells. *Joule* **2018**, *2*, 2450−2463.

(24) Sanehira, E. M.; Marshall, A. R.; Christians, J. A.; Harvey, S. P.; Ciesielski, P. N.; Wheeler, L. M.; Schulz, P.; Lin, L. Y.; Beard, M. C.; Luther, J. M. Enhanced Mobility $CsPbI_3$ Quantum Dot Arrays for

Record-Efficiency, High-Voltage Photovoltaic Cells. *Sci. Adv.* **2017**, *3*, 2375−2548.
(25) Suri, M.; Hazarika, A.; Larson, B. W.; Zhao, Q.; Vallés-Pelarda, M.; Siegler, T. D.; Abney, M. K.; Ferguson, A. J.; Korgel, B. A.; Luther, J. M. Enhanced Open-Circuit Voltage of Wide-Bandgap Perovskite Photovoltaics by Using Alloyed $(FA_{1-x}Cs_x)Pb(I_{1-x}Br_x)_3$ Quantum Dots. *ACS Energy Lett.* **2019**, *4*, 1954−1960.
(26) Ling, X.; Yuan, J.; Zhang, X.; Qian, Y.; Zakeeruddin, S. M.; Larson, B. W.; Zhao, Q.; Shi, J.; Yang, J.; Ji, K.; et al. Guanidinium-Assisted Surface Matrix Engineering for Highly Efficient Perovskite Quantum Dot Photovoltaics. *Adv. Mater.* **2020**, *32*, 2001906.
(27) Chen, K.; Jin, W.; Zhang, Y.; Yang, T.; Reiss, P.; Zhong, Q.; Bach, U.; Li, Q.; Wang, Y.; Zhang, H.; et al. High Efficiency Mesoscopic Solar Cells Using $CsPbI_3$ Perovskite Quantum Dots Enabled by Chemical Interface Engineering. *J. Am. Chem. Soc.* **2020**, *142*, 3775−3783.
(28) Zhao, Q.; Hazarika, A.; Chen, X.; Harvey, S. P.; Larson, B. W.; Teeter, G. R.; Liu, J.; Song, T.; Xiao, C.; Shaw, L.; et al. High Efficiency Perovskite Quantum Dot Solar Cells with Charge Separating Heterostructure. *Nat. Commun.* **2019**, *10*, 2842.
(29) Hao, M.; Bai, Y.; Zeiske, S.; Ren, L.; Liu, J.; Yuan, Y.; Zarrabi, N.; Cheng, N.; Ghasemi, M.; Chen, P.; et al. Ligand-Assisted Cation-Exchange Engineering for High-Efficiency Colloidal $Cs_{1-x}FA_xPbI_3$ Quantum Dot Solar Cells with Reduced Phase Segregation. *Nat. Energy* **2020**, *5*, 79−88.
(30) Yuan, J.; Hazarika, A.; Zhao, Q.; Ling, X.; Moot, T.; Ma, W.; Luther, J. M. Metal Halide Perovskites in Quantum Dot Solar Cells: Progress and Prospects. *Joule* **2020**, *4*, 1160−1185.
(31) Hazarika, A.; Zhao, Q.; Gaulding, E. A.; Christians, J. A.; Dou, B.; Marshall, A. R.; Moot, T.; Berry, J. J.; Johnson, J. C.; Luther, J. M. Perovskite Quantum Dot Photovoltaic Materials beyond the Reach of Thin Films: Full-Range Tuning of A-Site Cation Composition. *ACS Nano* **2018**, *12*, 10327−10337.
(32) Swarnkar, A.; Marshall, A. R.; Sanehira, E. M.; Chernomordik, B. D.; Moore, D. T.; Christians, J. A.; Chakrabarti, T.; Luther, J. M. Quantum Dot-Induced Phase Stabilization of α-$CsPbI_3$ Perovskite for High-Efficiency Photovoltaics. *Science* **2016**, *354*, 92−95.
(33) Wheeler, L. M.; Sanehira, E. M.; Marshall, A. R.; Schulz, P.; Suri, M.; Anderson, N. C.; Christians, J. A.; Nordlund, D.; Sokaras, D.; Kroll, T.; et al. Targeted Ligand-Exchange Chemistry on Cesium Lead Halide Perovskite Quantum Dots for High-Efficiency Photovoltaics. *J. Am. Chem. Soc.* **2018**, *140*, 10504−10513.
(34) Akkerman, Q. A.; Gandini, M.; Di Stasio, F.; Rastogi, P.; Palazon, F.; Bertoni, G.; Ball, J. M.; Prato, M.; Petrozza, A.; Manna, L. Strongly Emissive Perovskite Nanocrystal Inks for High-Voltage Solar Cells. *Nat. Energy* **2017**, *2*, 16194.
(35) Li, J.; Xu, L.; Wang, T.; Song, J.; Chen, J.; Xue, J.; Dong, Y.; Cai, B.; Shan, Q.; Han, B.; et al. 50-Fold EQE Improvement up to 6.27% of Solution-Processed All-Inorganic Perovskite $CsPbBr_3$ QLEDs via Surface Ligand Density Control. *Adv. Mater.* **2017**, *29*, 1603885.
(36) Zhang, X.; Xu, B.; Zhang, J.; Gao, Y.; Zheng, Y.; Wang, K.; Sun, X. W. All-Inorganic Perovskite Nanocrystals for High-Efficiency Light Emitting Diodes: Dual-Phase $CsPbBr_3$-$CsPb_2Br_5$ Composites. *Adv. Funct. Mater.* **2016**, *26*, 4595−4600.
(37) Chiba, T.; Hoshi, K.; Pu, Y.-J.; Takeda, Y.; Hayashi, Y.; Ohisa, S.; Kawata, S.; Kido, J. High-Efficiency Perovskite Quantum-Dot Light-Emitting Devices by Effective Washing Process and Interfacial Energy Level Alignment. *ACS Appl. Mater. Interfaces* **2017**, *9*, 18054−18060.
(38) Pan, J.; Quan, L. N.; Zhao, Y.; Peng, W.; Murali, B.; Sarmah, S. P.; Yuan, M.; Sinatra, L.; Alyami, N. M.; Liu, J.; et al. Highly Efficient Perovskite-Quantum-Dot Light-Emitting Diodes by Surface Engineering. *Adv. Mater.* **2016**, *28*, 8718−8725.
(39) Wang, P.; Bai, X.; Sun, C.; Zhang, X.; Zhang, T.; Zhang, Y. Multicolor Fluorescent Light-Emitting Diodes Based on Cesium Lead Halide Perovskite Quantum Dots. *Appl. Phys. Lett.* **2016**, *109*, No. 063106.
(40) Shi, Z.; Li, S.; Li, Y.; Ji, H.; Li, X.; Wu, D.; Xu, T.; Chen, Y.; Tian, Y.; Zhang, Y.; et al. Strategy of Solution-Processed All-Inorganic Heterostructure for Humidity/Temperature-Stable Perovskite Quantum Dot Light-Emitting Diodes. *ACS Nano* **2018**, *12*, 1462−1472.
(41) Huang, H.; Chen, B.; Wang, Z.; Hung, T. F.; Susha, A. S.; Zhong, H.; Rogach, A. L. Water Resistant $CsPbX_3$ Nanocrystals Coated with Polyhedral Oligomeric Silsesquioxane and Their Use as Solid State Luminophores in All-Perovskite White Light-Emitting Devices. *Chem. Sci.* **2016**, *7*, 5699−5703.
(42) Becker, M. A.; Vaxenburg, R.; Nedelcu, G.; Sercel, P. C.; Shabaev, A.; Mehl, M. J.; Michopoulos, J. G.; Lambrakos, S. G.; Bernstein, N.; Lyons, J. L.; et al. Bright Triplet Excitons in Caesium Lead Halide Perovskites. *Nature* **2018**, *553*, 189−193.
(43) Tsai, H.; Asadpour, R.; Blancon, J.-C.; Stoumpos, C. C.; Durand, O.; Strzalka, J. W.; Chen, B.; Verduzco, R.; Ajayan, P. M.; Tretiak, S.; et al. Light-Induced Lattice Expansion Leads to High-Efficiency Perovskite Solar Cells. *Science* **2018**, *360*, 67−70.
(44) Rolston, N.; Bennett-Kennett, R.; Schelhas, L. T.; Luther, J. M.; Christians, J. A.; Berry, J. J.; Dauskardt, R. H. Comment on "Light-Induced Lattice Expansion Leads to High-Efficiency Perovskite Solar Cells. *Science* **2020**, *368*, eaay8691.
(45) Wang, H.; Zhang, X.; Sui, N.; Hu, Y.; Colvin, V. L.; Yu, W. W.; Zhang, Y. Photoluminescence Loss and Recovery of α-$CsPbI_3$ Quantum Dots Originated from Chemical Equilibrium Shift of Oleylammonium. *ACS Appl. Mater. Interfaces* **2020**, *12*, 11769−11777.
(46) Boote, B. W.; Andaraarachchi, H. P.; Rosales, B. A.; Blome-Fernández, R.; Zhu, F.; Reichert, M. D.; Santra, K.; Li, J.; Petrich, J. W.; Vela, J.; et al. Unveiling the Photo- and Thermal-Stability of Cesium Lead Halide Perovskite Nanocrystals. *ChemPhysChem* **2019**, *20*, 2647−2656.
(47) Yuan, G.; Ritchie, C.; Ritter, M.; Murphy, S.; Gómez, D. E.; Mulvaney, P. The Degradation and Blinking of Single $CsPbI_3$ Perovskite Quantum Dots. *J. Phys. Chem. C* **2018**, *122*, 13407−13415.
(48) Ruan, L. J.; Tang, B.; Shu, A.; Qin, C.; Ma, Y. Self-Passivation of $CsPbBr_3$ Nanocrystals through Introducing Bromide Vacancies and Ultraviolet Irradiation. *J. Phys. Chem. C* **2021**, *125*, 1010−1017.
(49) Zhang, Y.; Zhu, H.; Zheng, J.; Chai, G.; Song, Z.; Chen, Y.; Liu, Y.; He, S.; Shi, Y.; Tang, Y.; et al. Performance Enhancement of All-Inorganic Perovskite Quantum Dots ($CsPbX_3$) by UV-NIR Laser Irradiation. *J. Phys. Chem. C* **2019**, *123*, 4502−4511.
(50) Moyen, E.; Kanwat, A.; Cho, S.; Jun, H.; Aad, R.; Jang, J. Ligand Removal and Photo-Activation of $CsPbBr_3$ Quantum Dots for Enhanced Optoelectronic Devices. *Nanoscale* **2018**, *10*, 8591−8599.
(51) Shamsi, J.; Rastogi, P.; Caligiuri, V.; Abdelhady, A. L.; Spirito, D.; Manna, L.; Krahne, R. Bright-Emitting Perovskite Films by Large-Scale Synthesis and Photoinduced Solid-State Transformation of $CsPbBr_3$ Nanoplatelets. *ACS Nano* **2017**, *11*, 10206−10213.
(52) Seth, S.; Mondal, N.; Patra, S.; Samanta, A. Fluorescence Blinking and Photoactivation of All-Inorganic Perovskite Nanocrystals $CsPbBr_3$ and $CsPbBr_2I$. *J. Phys. Chem. Lett.* **2016**, *7*, 266−271.
(53) Zhang, Y.; Siegler, T. D.; Thomas, C. J.; Abney, M. K.; Shah, T.; De Gorostiza, A.; Greene, R. M.; Korgel, B. A. A "Tips and Tricks" Practical Guide to the Synthesis of Metal Halide Perovskite Nanocrystals. *Chem. Mater.* **2020**, *32*, 5410−5423.
(54) Thomas, C. J.; Zhang, Y.; Guillaussier, A.; Bdeir, K.; Aly, O. F.; Kim, H. G.; Noh, J.; Reimnitz, L. C.; Li, J.; Deepak, F. L.; et al. Thermal Stability of the Black Perovskite Phase in Cesium Lead Iodide Nanocrystals Under Humid Conditions. *Chem. Mater.* **2019**, *31*, 9750−9758.
(55) Marronnier, A.; Roma, G.; Boyer-Richard, S.; Pedesseau, L.; Jancu, J.-M.; Bonnassieux, Y.; Katan, C.; Stoumpos, C. C.; Kanatzidis, M. G.; Even, J. Anharmonicity and Disorder in the Black Phases of Cesium Lead Iodide Used for Stable Inorganic Perovskite Solar Cells. *ACS Nano* **2018**, *12*, 3477−3486.
(56) Bertolotti, F.; Protesescu, L.; Kovalenko, M. V.; Yakunin, S.; Cervellino, A.; Billinge, S. J. L.; Terban, M. W.; Pedersen, J. S.; Masciocchi, N.; Guagliardi, A. Coherent Nanotwins and Dynamic

https://doi.org/10.1021/acs.jpcc.2c04305
J. Phys. Chem. C 2022, 126, 12712−12720

Disorder in Cesium Lead Halide Perovskite Nanocrystals. *ACS Nano* **2017**, *11*, 3819−3831.
(57) Sutton, R. J.; Filip, M. R.; Haghighirad, A. A.; Sakai, N.; Wenger, B.; Giustino, F.; Snaith, H. J. Cubic or Orthorhombic? Revealing the Crystal Structure of Metastable Black-Phase $CsPbI_3$ by Theory and Experiment. *ACS Energy Lett.* **2018**, *3*, 1787−1794.
(58) Zhao, B.; Jin, S.-F.; Huang, S.; Liu, N.; Ma, J.-Y.; Xue, D.-J.; Han, Q.; Ding, J.; Ge, Q.-Q.; Feng, Y.; et al. Thermodynamically Stable Orthorhombic γ-$CsPbI_3$ Thin Films for High-Performance Photovoltaics. *J. Am. Chem. Soc.* **2018**, *140*, 11716−11725.
(59) Straus, D. B.; Guo, S.; Cava, R. J. Kinetically Stable Single Crystals of Perovskite-Phase $CsPbI_3$. *J. Am. Chem. Soc.* **2019**, *141*, 11435.
(60) Makarov, N. S.; Guo, S.; Isaienko, O.; Liu, W.; Robel, I.; Klimov, V. I. Spectral and Dynamical Properties of Single Excitons, Biexcitons, and Trions in Cesium−Lead-Halide Perovskite Quantum Dots. *Nano Lett.* **2016**, *16*, 2349−2362.
(61) Mondal, N.; Samanta, A. Complete Ultrafast Charge Carrier Dynamics in Photo-Excited All-Inorganic Perovskite Nanocrystals ($CsPbX_3$). *Nanoscale* **2017**, *9*, 1878−1885.
(62) Li, J.; Yuan, X.; Jing, P.; Li, J.; Wei, M.; Hua, J.; Zhao, J.; Tian, L. Temperature-Dependent Photoluminescence of Inorganic Perovskite Nanocrystal Films. *RSC Adv.* **2016**, *6*, 78311−78316.
(63) Sillen, A.; Engelborghs, Y. The Correct Use of "Average" Fluorescence Parameters. *Photochem. Photobiol.* **1998**, *67*, 475−486.
(64) Diroll, B. T.; Zhou, H.; Schaller, R. D. Low-Temperature Absorption, Photoluminescence, and Lifetime of $CsPbX_3$ (X = Cl, Br, I) Nanocrystals. *Adv. Funct. Mater.* **2018**, *28*, 1800945.
(65) Busipalli, D. L.; Lin, K.-Y.; Nachimuthu, S.; Jiang, J.-C. Enhanced Moisture Stability of Cesium Lead Iodide Perovskite Solar Cells—a First-Principles Molecular Dynamics Study. *Phys. Chem. Chem. Phys.* **2020**, *22*, 5693−5701.
(66) Tian, Y.; Peter, M.; Unger, E.; Abdellah, M.; Zheng, K.; Pullerits, T.; Yartsev, A.; Sundström, V.; Scheblykin, I. G. Mechanistic Insights into Perovskite Photoluminescence Enhancement: Light Curing with Oxygen Can Boost Yield Thousandfold. *Phys. Chem. Chem. Phys.* **2015**, *17*, 24978−24987.
(67) Brenes, R.; Guo, D.; Osherov, A.; Noel, N. K.; Eames, C.; Hutter, E. M.; Pathak, S. K.; Niroui, F.; Friend, R. H.; Islam, M. S.; et al. Metal Halide Perovskite Polycrystalline Films Exhibiting Properties of Single Crystals. *Joule* **2017**, *1*, 155−167.
(68) Feng, X.; Su, H.; Wu, Y.; Wu, H.; Xie, J.; Liu, X.; Fan, J.; Dai, J.; He, Z. Photon-Generated Carriers Excite Superoxide Species Inducing Long-Term Photoluminescence Enhancement of $MAPbI_3$ Perovskite Single Crystals. *J. Mater. Chem. A* **2017**, *5*, 12048−12053.
(69) Brenes, R.; Eames, C.; Bulović, V.; Islam, M. S.; Stranks, S. D. The Impact of Atmosphere on the Local Luminescence Properties of Metal Halide Perovskite Grains. *Adv. Mater.* **2018**, *30*, 1706208.
(70) Galisteo-López, J. F.; Anaya, M.; Calvo, M. E.; Míguez, H. Environmental Effects on the Photophysics of Organic−Inorganic Halide Perovskites. *J. Phys. Chem. Lett.* **2015**, *6*, 2200−2205.
(71) Kheraj, V.; Simonds, B. J.; Toshniwal, A.; Misra, S.; Peroncik, P.; Zhang, C.; Vardeny, Z. V.; Scarpulla, M. A. Using Photoluminescence to Monitor the Optoelectronic Properties of Methylammonium Lead Halide Perovskites in Light and Dark over Periods of Days. *J. Lumin.* **2018**, *194*, 353−358.
(72) Motti, S. G.; Gandini, M.; Barker, A. J.; Ball, J. M.; Srimath Kandada, A. R.; Petrozza, A. Photoinduced Emissive Trap States in Lead Halide Perovskite Semiconductors. *ACS Energy Lett.* **2016**, *1*, 726−730.
(73) Fang, H.-H.; Adjokatse, S.; Wei, H.; Yang, J.; Blake, G. R.; Huang, J.; Even, J.; Loi, M. A. Ultrahigh Sensitivity of Methylammonium Lead Tribromide Perovskite Single Crystals to Environmental Gases. *Sci. Adv.* **2016**, *2*, e1600534.
(74) Knight, A. J.; Wright, A. D.; Patel, J. B.; McMeekin, D. P.; Snaith, H. J.; Johnston, M. B.; Herz, L. M. Electronic Traps and Phase Segregation in Lead Mixed-Halide Perovskite. *ACS Energy Lett.* **2019**, *4*, 75−84.
(75) Lu, D.; Zhang, Y.; Lai, M.; Lee, A.; Xie, C.; Lin, J.; Lei, T.; Lin, Z.; Kley, C. S.; Huang, J.; et al. Giant Light-Emission Enhancement in Lead Halide Perovskites by Surface Oxygen Passivation. *Nano Lett.* **2018**, *18*, 6967−6973.
(76) Wang, K.; Gao, C.; Xu, Z.; Tian, Q.; Gu, X.; Zhang, L.; Zhang, S.; Zhao, K.; Liu, S. F. In-Situ Hot Oxygen Cleansing and Passivation for All-Inorganic Perovskite Solar Cells Deposited in Ambient to Breakthrough 19% Efficiency. *Adv. Funct. Mater.* **2021**, *31*, 2101568.
(77) Ghosh, P.; Farooq, U.; Su, H.; Pei, S.; Li, G.; He, W.; Dai, J.; Huang, L.; Huang, M. Strain-Induced Light Emission Enhancement in CsPbBr3Microwires. *J. Mater. Sci.* **2022**, *57*, 5061−5071.
(78) Wang, Y.; Ren, Y.; Zhang, S.; Wu, J.; Song, J.; Li, X.; Xu, J.; Sow, C. H.; Zeng, H.; Sun, H. Switching Excitonic Recombination and Carrier Trapping in Cesium Lead Halide Perovskites by Air. *Commun. Phys.* **2018**, *1*, 1−8.
(79) Valeur, B.; Berberan-Santos, M. N. *Molecular Fluorescence: Principles and Applications*; Wiley-VCH Verlag GmbH & Co. KGaA: Weinheim, Germany, 2012.
(80) Lakowicz, J. R. *Principles of Fluorescence Spectroscopy*; Springer: New York, 2010.
(81) Korgel, B. A.; Fullam, S.; Connolly, S.; Fitzmaurice, D. Assembly and Self-Organization of Silver Nanocrystal Superlattices: Ordered 'Soft Spheres'. *J. Phys. Chem. B* **1998**, *102*, 8379−8388.
(82) Zhang, J.; Zhao, W.; Olthof, S.; Liu, S. F. Defects in $CsPbX_3$ Perovskite: From Understanding to Effective Manipulation for High-Performance Solar Cells. *Small Methods* **2021**, *5*, 2100725.
(83) Liu, Y.; Palotas, K.; Yuan, X.; Hou, T.; Lin, H.; Li, Y.; Lee, S.-T. Atomistic Origins of Surface Defects in $CH_3NH_3PbBr_3$ Perovskite and Their Electronic Structures. *ACS Nano* **2017**, *11*, 2060−2065.
(84) Lin, J.; Lai, M.; Dou, L.; Kley, C. S.; Chen, H.; Peng, F.; Sun, J.; Lu, D.; Hawks, S. A.; Xie, C.; et al. Thermochromic Halide Perovskite Solar Cells. *Nat. Mater.* **2018**, *17*, 261−267.
(85) Liu, S.-C.; Li, Z.; Yang, Y.; Wang, X.; Chen, Y.-X.; Xue, D.-J.; Hu, J.-S. Investigation of Oxygen Passivation for High-Performance All-Inorganic Perovskite Solar Cells. *J. Am. Chem. Soc.* **2019**, *141*, 18075−18082.
(86) Hanrath, T.; Korgel, B. A. Influence of Surface States on Electron Transport through Intrinsic Ge Nanowires. *J. Phys. Chem. B* **2005**, *109*, 5518−5524.

https://doi.org/10.1021/acs.jpcc.2c04305
J. Phys. Chem. C 2022, 126, 12712−12720